AGU PUBLICATIONS

JGR

Journal of Geophysical Research: Space Physics

RESEARCH ARTICLE
10.1002/2015JA021180

Key Points:
- Observe seasonal variation in equatorial electron densities inside 3.25 R_s
- Seasonal variation diminishes with distance from Saturn, vanishing beyond 4.0 R_s
- Observe evidence for propagation of ring plasma near inner edge of E Ring

Correspondence to:
A. M. Persoon,
ann-persoon@uiowa.edu

Citation:
Persoon, A. M., D. A. Gurnett, W. S. Kurth, J. B. Groene, and J. B. Faden (2015), Evidence for a seasonally dependent ring plasma in the region between Saturn's A Ring and Enceladus' orbit, *J. Geophys. Res. Space Physics*, *120*, 6276–6285, doi:10.1002/2015JA021180.

Received 3 MAR 2015
Accepted 18 JUL 2015
Accepted article online 22 JUL 2015
Published online 17 AUG 2015

Evidence for a seasonally dependent ring plasma in the region between Saturn's A Ring and Enceladus' orbit

A. M. Persoon[1], D. A. Gurnett[1], W. S. Kurth[1], J. B. Groene[1], and J. B. Faden[1]

[1]Department of Physics and Astronomy, University of Iowa, Iowa City, Iowa, USA

Abstract Equatorial electron density measurements from the Cassini Radio and Plasma Wave Science experiment are derived from the upper hybrid resonance frequency from Saturn Orbit Insertion (SOI) on 1 July 2004 through 21 May 2013. These densities are used to determine the characteristics of the plasma in the inner magnetosphere of Saturn between the outer edge of the A Ring and the orbit of Enceladus. Electron densities obtained when Cassini first arrived at Saturn on 1 July 2004 showed a plasma distribution decreasing radially outward from Saturn in the direction of Enceladus, the expected distribution of a centrifugally driven plasma expanding radially outward from a source in the main rings. We examine equatorial electron densities in the region between 2.4 and 4.0 R_s and show that the density measurements in this region exhibit a strong seasonal dependence resulting from photon-induced decomposition of icy particles on the ring surfaces, a decomposition process which is controlled by the solar incidence angle. This seasonal dependence will have plasma density implications for Cassini when the spacecraft returns to the region just beyond the A Ring in 2016.

1. Introduction

The plasma in Saturn's inner magnetosphere has many potential sources. In the region between 2.4 and 4.0 Saturnian radii (R_s), two are of primary interest: the plasma source at the icy moon Enceladus and the plasma source in the atmosphere of the main rings. Other possible sources include the tiny moons and the narrow and tenuous arcs and rings in this region. These are not expected to be significant sources of Saturn's magnetospheric plasma.

As early as the Pioneer/Voyager era, Saturn's main rings were believed to be an important source of plasma and neutrals in the main ring system and in the plasma torus beyond the rings [*Frank et al*., 1980; *Wilson and Waite*, 1989]. Photodissociation of the icy ring particles, ion-induced sputtering, and micrometeorite bombardment were all believed to contribute to the decomposition of the icy particles on the ring surfaces and the creation of the ring atmosphere [*Carlson*, 1980; *Frank et al*., 1980; *Morfill et al*., 1983; *Johnson et al*., 1989; *Wilson and Waite*, 1989; *Pospieszalska and Johnson*, 1991; *Ip*, 1995]. Cassini measurements of neutrals and ions over the ring system have confirmed the importance of the main rings as a source of neutrals and plasma in Saturn's magnetosphere. H_2 [*Tseng et al*., 2011] and O_2, the main atmospheric constituent [*Tseng et al*., 2010], are released into the ring atmosphere through the decomposition of icy ring particles by UV photons [*Ip*, 1995; *Waite et al*., 2005; *Young et al*., 2005; *Johnson et al*., 2006a], suggesting that photodissociation is the primary decomposition process acting on the ring particles. Subsequent photoionization of these molecules in the ring atmosphere creates a thin layer of ionospheric plasma in the main ring system [*Gurnett et al*., 2005; *Tokar et al*., 2005; *Wahlund et al*., 2005; *Waite et al*., 2005; *Young et al*., 2005]. Photodissociated oxygen molecules from the ring atmosphere are also scattered, possibly by micrometeorite bombardment [*Pospieszalska and Johnson*, 1991] or by ion-molecule collisions [*Ip*, 2005; *Johnson et al*., 2006a; *Tseng et al*., 2010], into the extended ring atmosphere beyond the A Ring and are subsequently ionized, providing a source of ring plasma in the region beyond the outer edge of the A Ring at 2.3 R_s.

In the years between the Voyager flybys of Saturn and the arrival of Cassini at Saturn, efforts were made to calculate flux rates from the decomposition of ice by sputtering and meteoroid impacts on the main rings as well as the icy moons and more tenuous rings, but the results were inadequate to account for the large neutral cloud observed by the Hubble Space Telescope [*Shemansky et al*., 1993; *Shi et al*., 1995;

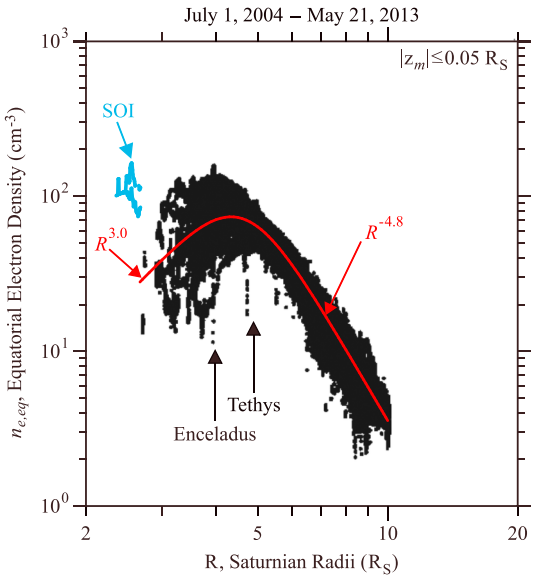

Figure 1. A radial profile of all RPWS electron density measurements within 0.05 R_S of the magnetic equatorial plane from 1 July 2004 to 21 May 2013. The densities beyond 3 R_S show the typical distribution of the Enceladus plasma, with plasma diffusing both inward and outward from a broad density peak just beyond the Enceladus orbit. The red line in Figure 1 is a power law fit to the bin-averaged density measurements derived from the radial dependence model of *Persoon et al.* [2013]. The density measurements obtained as Cassini moved outward from the main rings on 1 July 2004 (SOI) show the distribution of the ring plasma as it diffuses outward from a source in the main rings.

Richardson et al., 1998; *Jurac et al.*, 2001]. An additional water source in the vicinity of Enceladus was needed, and Cassini found it during two close flybys of the icy moon in 2005. Water and ice molecules were discovered to be venting from the moon's southern polar region [*Dougherty et al.*, 2006; *Hansen et al.*, 2006; *Porco et al.*, 2006; *Waite et al.*, 2006]. Through neutral-neutral collisions, charge-exchange interactions, and ion-neutral collisions, the water molecules and their dissociated water group neutrals are scattered into the vast neutral torus of Saturn's magnetosphere [*Jurac et al.*, 2002; *Jurac and Richardson*, 2005; *Johnson et al.*, 2006b; *Farmer*, 2009; *Hartogh et al.*, 2011; *Cassidy and Johnson*, 2010]. The ionization of these neutrals is the source of the Enceladus plasma. One of Cassini's greatest achievements is the discovery that the geysers of Enceladus are the dominant source of plasma in Saturn's magnetosphere (see review by *Arridge et al.* [2012]).

This study will build on the equatorial electron density database used in *Persoon et al.* [2013] to investigate equatorial electron distributions from different plasma sources in the inner magnetosphere. We use the Radio and Plasma Wave Science (RPWS) equatorial electron density measurements derived from the upper hybrid emissions from 1 July 2004 to 21 May 2013 to illustrate the electron distributions characteristic of plasma from a source at Enceladus and from the main ring system and to study seasonal effects on the ring plasma in the inner magnetosphere. To minimize latitudinal variations, we define the equatorial densities to be those measurements within 0.05 R_s of Saturn's magnetic equatorial plane.

2. Distribution Characteristics for Two Plasma Populations

Electron density measurements from the Cassini Radio and Plasma Wave Science (RPWS) experiment, from the RPWS/Langmuir Probe instrument (RPWS/LP), and from the Electron Spectrometer of the Cassini Plasma Spectrometer (CAPS/ELS) have been used to map the electron distribution from 3 R_s to 10 R_s and beyond [*Persoon et al.*, 2006, 2009, 2013; *Schippers et al.*, 2008, 2013; *Sittler et al.*, 2008; *Morooka et al.*, 2009]. After statistical binning and averaging for 7 years of density measurements, *Persoon et al.* [2013] found that the equatorial electrons have a density distribution slightly offset from Enceladus with a broad peak from 4 R_s to 5 R_s. The density increases radially outward from Saturn as $R^{4.0}$ between 3 R_s and 4 R_s and falls off with increasing distance as $R^{-4.8}$ outside 5 R_s (see Figure 3 in *Persoon et al.* [2013]). A similar electron distribution was observed in the RPWS/LP and CAPS/ELS electron density data beyond 5 R_s [*Schippers et al.*, 2008, 2013; *Morooka et al.*, 2009], in the equatorial electron density model for Saturn's inner magnetosphere beyond 3 R_s derived by *Sittler et al.* [2008] and in the RPWS/LP ion distribution between 2.4 and 12 R_s [*Holmberg et al.*, 2012]. This distribution is characteristic of a plasma that is radially diffusing both inward and outward from the plasma source at Enceladus.

The characteristic distribution of the Enceladus plasma is seen for 94% of the equatorial orbits for which there are RPWS density measurements inside the Enceladus orbit [*Persoon et al.*, 2005, 2013]. Figure 1 is a radial profile of all RPWS equatorial densities from 1 July 2004 to 21 May 2013 for measurements within 0.05 R_s of the magnetic equatorial plane. It can be easily seen that the density profiles beyond 5 R_s are consistently repeatable with a spread in the densities of ~30%. But inside 4 R_s the density distribution is

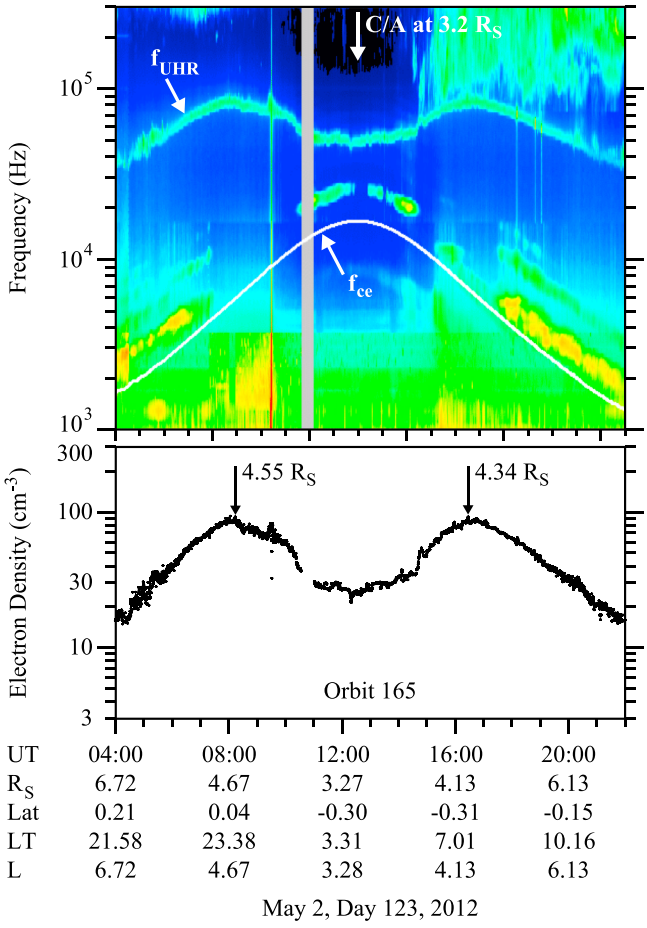

Figure 2. (top) An electric field spectrogram and (bottom) an electron density profile of a Cassini pass through the inner magnetosphere on 2 May 2012. This density profile illustrates the typical Enceladus plasma distribution where the density peaks on the inbound and outbound segments at 4.55 and 4.34 R_s, respectively. Inside the density peak region the densities roll off, forming a density trough centered on closest approach (C/A).

highly variable with a spread that is nearly twice as large. The red line in Figure 1 is a power law fit to the equatorial density measurements which have been averaged in radial bins of 0.2 R_s. The bin-averaged equatorial electron density measurements have been fit to the hybrid power law equation from the radial dependence model derived by *Persoon et al.* [2013]:

$$n^*_{e,\mathrm{eq}} = \frac{n_0}{\frac{1}{2}\left[\left(\frac{R_0}{R}\right)^m + \left(\frac{R}{R_0}\right)^n\right]} \quad (1)$$

where $n^*_{e,\mathrm{eq}}$ refers to the model equatorial electron density, n_0 is the density at the peak of the distribution, R_0 is the radial distance of the peak, and m and n are the radial dependencies of the electron distribution inside and outside the density peak, respectively. A comparison between the fit shown in Figure 1 and the radial dependence model in *Persoon et al.* [2013] shows the same broad density peak between the orbits of Enceladus and Tethys, with the same peak density of 72 cm^{-3} at the same radial distance of 4.6 R_s. Beyond 5 R_s, the radial dependence of the plasma distribution also remains the same with the plasma decreasing radially outward as $R^{-4.8}$ ($n = 4.8$) beyond 5 R_s. Inside 4 R_s, the densities are again increasing radially outward from Saturn toward the plasma source at Enceladus. However, the slope of the electron distribution is now reduced to $R^{3.0}$ ($m = 3.0$) due to the addition of enhanced electron densities inside the orbit of Enceladus in late 2011/early 2012 (see Figure 4).

Not all of the electron density profiles inside the orbit of Enceladus show the same R^3 dependence. *Gurnett et al.* [2005] identified a large density depletion over the main rings and a 2 order of magnitude increase in the electron density measurements at the outer edge of the A Ring (see Figure 5 in *Gurnett et al.* [2005]). Also shown in Figure 1 is a radial density profile of the Saturn Orbit Insertion (SOI) equatorial density measurements (in blue) obtained within 0.05 R_s of the magnetic equatorial plane at radial distances of 2.4 to 2.7 R_s in the region just beyond the A Ring. These densities decrease with increasing distance from Saturn suggestive of a centrifugally driven plasma diffusing outward from a source in the main rings.

SOI currently provides the only electron density measurements in the region just beyond the A Ring, but there are 32 equatorial orbits that provide RPWS electron density measurements in the region inside 4 R_s. Twenty seven of these orbits have a well-defined electron density peak just beyond Enceladus' orbit and the densities roll-off inside the density peak. Figure 2 is a typical example of the Enceladus plasma distribution. The top plot is an RPWS electric field spectrogram for a Cassini pass on 2 May 2012. The solid white line is the electron cyclotron frequency (f_{ce}) derived from the magnetic field measurements. Above the f_{ce} line are the upper hybrid resonance frequency (f_{UHR}) emissions from which the electron densities

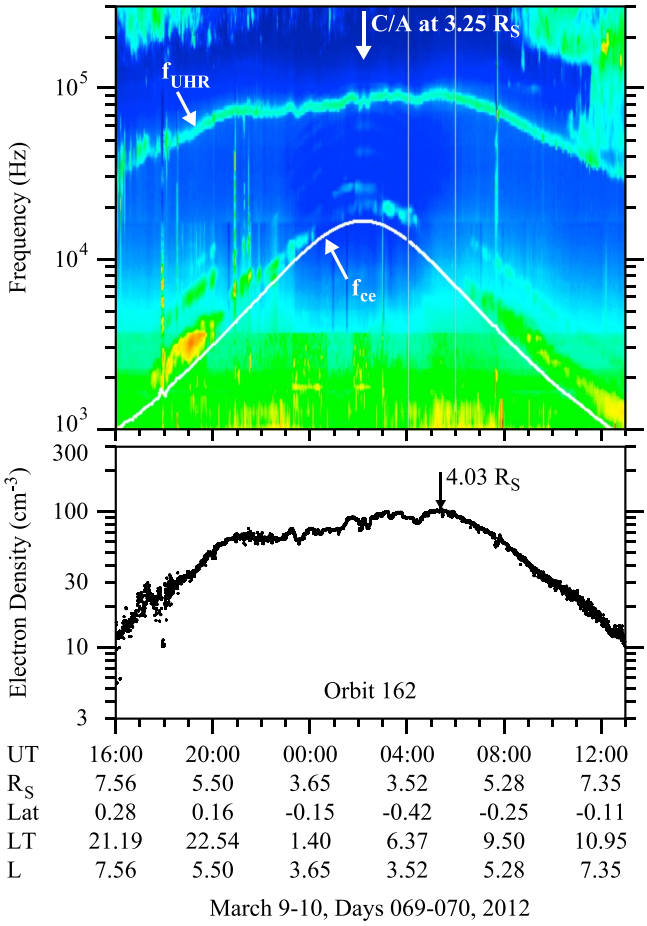

Figure 3. (top) An electric field spectrogram and (bottom) an electron density profile of a Cassini pass through the inner magnetosphere on 9 and 10 May 2012. This density profile does not show the expected density roll-off inside the Enceladus orbit. The density peaks at 4.03 R_S during the outbound portion of the orbit but there is no peak in the inbound density profile. In the region inside 4 R_S, the density trough appears to be nearly filled in, suggesting that plasma has been added to the system in this region.

are derived [*Persoon et al.*, 2005]. Cassini's closest approach (C/A) to Saturn occurs at 12:33 UT when the spacecraft is at 3.2 R_S, just inside the inner edge of the E Ring. The bottom plot in Figure 2 is the electron density-time profile for the same time interval. The density profile clearly shows an Enceladus density peak on the inbound orbital segment at 08:14 UT and a second density peak on the outbound orbital segment at 16:27 UT, when Cassini was at 4.6 and 4.3 R_S, respectively. Inside the density peaks, the density falls off with increasing distance from the Enceladus source, creating the appearance of a density "trough" centered on closest approach.

The remaining five orbits with electron density measurements inside 4 R_S show evidence of the trough being partially or completely filled in. Figure 3 has the same format as Figure 2 and illustrates the electric field spectrogram and electron density-time profile for the orbit on 9 and 10 March 2012. Closest approach occurs at 02:13 UT when Cassini was at 3.3 R_S. There is a density peak during the outbound portion of the orbit at 4.03 R_S and a slight roll-off just inside this peak but there is no peak in the inbound density profile. The density trough is nearly filled in.

Figure 4 illustrates the radial density profiles for the five orbits showing evidence of a filled-in density trough, superimposed on the electron density distribution in Figure 1. The five density profiles are not typical of the Enceladus plasma distribution inside Enceladus' orbit and highlight the dynamic nature of the plasma chemistry in the inner magnetosphere. Possible dust-charging effects in the E Ring region need to be investigated. Elevated densities also suggest a local enhancement in the Enceladus plasma production and/or an enhancement in the ring plasma production and subsequent transport of the ring plasma into this region to merge with the Enceladus plasma.

3. Seasonal Variability of Ring Plasma

When the Cassini spacecraft passed above the dark side of the rings on 1 July 2004, the instruments detected an enhancement in the electron density over the Cassini division [*Coates et al.*, 2005; *Wahlund et al.*, 2005; *Young et al.*, 2005; *Farrell et al.*, 2008] and an inverse correlation between the electron density measurements and the opacity of the B Ring and the A Ring [*Esposito et al.*, 1983; *Coates et al.*, 2005; *Young et al.*, 2005], suggesting that a photon-induced decomposition process was acting on the icy ring particles on the sunlit surface of the rings, creating the ring atmosphere. The photodissociated oxygen molecules in the atmosphere [*Bouhram et al.*, 2006; *Johnson et al.*, 2006a] are subsequently photoionized

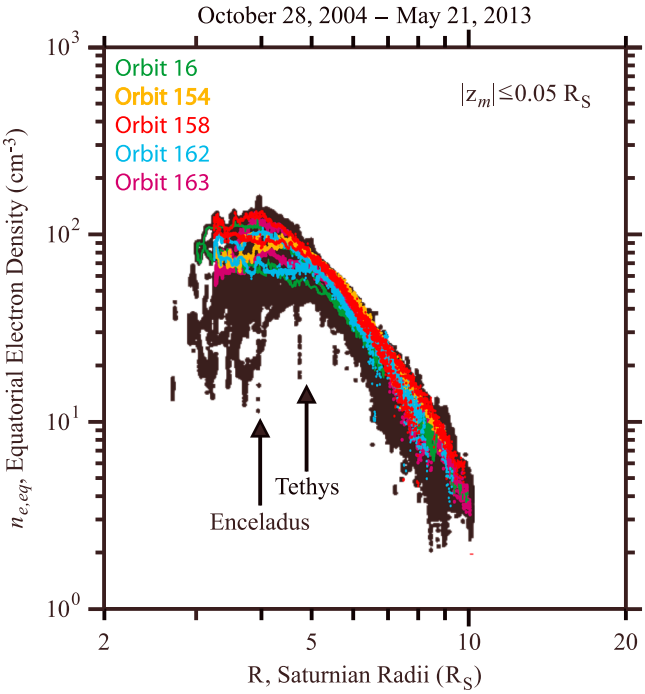

Figure 4. Radial density profiles for five orbits showing evidence of enhanced densities and a filled-in density trough inside Enceladus' orbit, superimposed on the electron density distribution in Figure 1. These density profiles are evidence of the dynamic nature of plasma production and transport in the inner magnetosphere.

to create the tenuous ring ionosphere, dominated by O_2^+ and O^+ ions [*Coates et al.*, 2005; *Gurnett et al.*, 2005; *Tokar et al.*, 2005; *Young et al.*, 2005]. Ion and electron densities in the ring ionosphere are 2 orders of magnitude lower than the densities measured just beyond the outer edge of the A Ring [*Gurnett et al.*, 2005; *Young et al.*, 2005; *Farrell et al.*, 2008]. The low plasma densities in the ring ionosphere are believed to be due to plasma absorption by the ring particles and diminished photodissociation of the icy particles on the shadowed ring surface during the outbound portion of SOI [*Wahlund et al.*, 2005]. The very high plasma densities seen just beyond the outer edge of the A Ring result from the photoionization of the photodissociated water group neutrals which, by ion-molecule collisions, have scattered outward into an extended ring atmosphere in the region beyond the main rings [*Ip*, 2005; *Johnson et al.*, 2006a].

Photon-induced decomposition of icy ring particles would indicate that the source rate of the photodissociated neutrals in the ring atmosphere and beyond would vary with the incident angle of the Sun on the ring surfaces [*Tseng et al.*, 2010], subsequently affecting the ionization process in the region beyond the A Ring. The top plot in Figure 5 illustrates the angle of the Sun above/below Saturn's equatorial plane for one seasonal cycle. In the bottom plot are the equatorial density measurements inside 3.25 R_S derived from both equatorial orbits and the equatorial portion of high-inclination orbits. The densities are binned in 3 month increments and averaged (black dots). Cassini arrived at Saturn in mid-2004, nearly 2 years after the southern summer solstice. The equatorial electron densities measured during Cassini's first orbit were some of the highest densities measured outside the main ring system. The lowest averaged equatorial electron densities were measured in the year preceding the Saturn equinox (11 August 2009), when the rings were edge-on to the Sun and photon-induced decomposition of the icy ring particles would be restricted by the low solar incident angle of the Sun on the ring surfaces. Density measurements in 2012 are again increasing as Saturn approaches the midpoint between the equinox and the northern summer solstice. The solid red line represents a cosine fit through the bin-averaged data points. The density value from the fit is given by

$$n_e = -A\cos\left(360\frac{(t-t_0)}{T}+\phi\right)+C \tag{2}$$

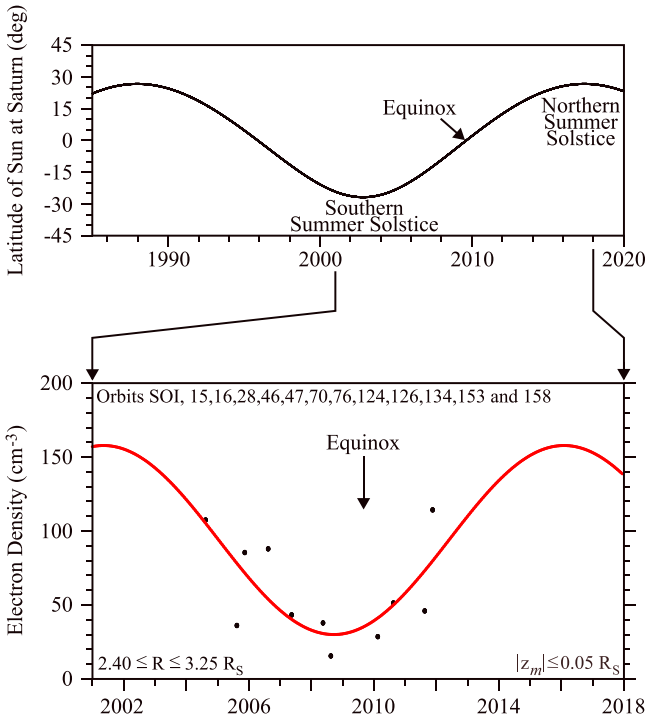

Figure 5. The top plot illustrates the angle of the Sun above/below the equatorial plane for one full seasonal cycle. The bottom plot shows the RPWS equatorial electron density measurements between 2.40 R_S and 3.25 R_S, binned in 3 month increments and averaged. A cosine fit through the averaged points (solid red line) shows a strong seasonal effect, with a density depletion 10 months before the 2009 equinox and densities increasing toward the summer solstices.

where A and C are the cosine-wave amplitude and offset, respectively, ϕ is the phase in degrees measured from the Saturnian equinox (11 August, 2009), t_0 is the time of the 2009 equinox in years, t is the time of the averaged density value in years, and the period T is 14.73 years, half of Saturn's rotational period which includes the 2002 southern summer solstice and the 2017 northern summer solstice. Although there is a lot of scatter in the data, the cosine fit shows a density minimum 10 months before the 2009 equinox with densities increasing toward the summer solstices. The fit is in good qualitative agreement with the seasonal effect seen in the thermal ion distribution at $L = 3$ by *Elrod et al*. [2014].

Figure 6 is a multipanel plot of the equatorial electron density measurements inside 5.25 R_S, grouped in bins of 0.5 R_S. All of the measurements have been averaged in 3 month increments. The top plot reproduces the averaged data points and the cosine fit for the electron density measurements inside 3.25 R_S, shown in Figure 5. The 0.85 R_S radial bin for the top plot is greater than the 0.5 R_S bins for the lower four plots because of the reduced number of electron density measurements inside 3.25 R_S. The radial bin has been expanded to accumulate sufficient density measurements over the 9 year time interval to provide a reasonable fit to the data. The cosine fit to the data for each panel in Figure 6 is shown in red.

The coefficients for the cosine fits are listed in Table 1. The highest amplitude of the seasonal variation on the density distribution occurs inside 3.25 R_S. Beyond 3.25 R_S, the amplitude and cosine wave offset (A and C in Table 1) fall significantly with increasing radial distance. As the amplitude continues to diminish with increasing radial distance, the cosine fit approaches a straight line beyond 4.25 R_S where the seasonal dependence vanishes. The uncertainty in the phase coefficient φ is lowest inside 3.25 R_S and increases with increasing radial distance. Beyond 4.25 R_S where the cosine fit tends to a straight line, the phase cannot be determined with reasonable certainty, indicated by the *** in Table 1. The uncertainty in the cosine fit to the density measurements (the last column in Table 1) is largest in the first radial bin, due to the large variability in the density measurements and the fewer number of density measurements inside 3.25 R_S. The uncertainty falls with increasing radial distance as the spread in the density measurements diminishes and the number of density measurements increases. Beyond 4.25 R_S, the uncertainty in the cosine fit is equal to or greater than the amplitude of the fit, which now approaches a straight line.

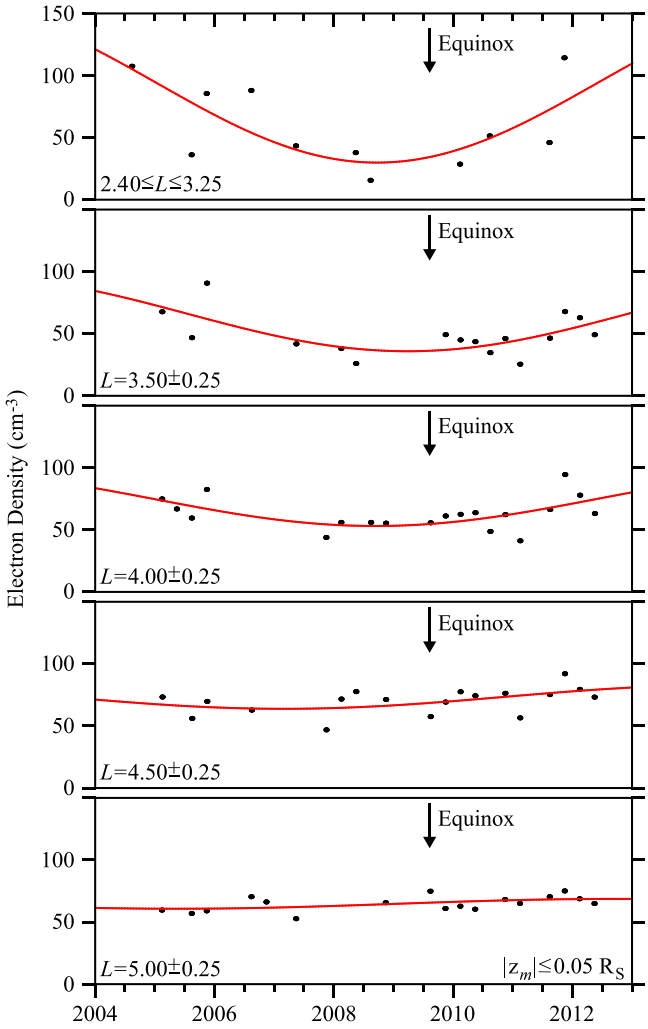

Figure 6. These five panels show the RPWS equatorial electron densities averaged in 3 month increments and grouped in bins of 0.5 R_S. The top plot reproduces the averaged data points and the cosine fit for the electron density measurements inside 3.25 R_S, shown in Figure 5. The 0.85 R_S radial bin for the top plot is greater than the 0.5 R_S bins for the lower four plots to accommodate the reduced number of electron density measurements in this bin and to provide a reasonable fit to the data. Cosine fits through the averaged data points (red lines) show that there is a strong seasonal variability inside 3.25 R_S (Figure 6, top). This seasonal dependence becomes negligible beyond the Enceladus orbit (fourth and fifth panels).

Because the seasonal variation grows weaker with increasing distance from the rings, disappearing beyond the orbit of Enceladus, we propose that the seasonal dependence observed inside 4 R_S is a marker identifying the presence of the ring plasma in this region. The maximum spread in the density measurements during this 9 year time interval due to a seasonal dependence is much less than the order of magnitude spread in the density measurements observed inside 4 R_S in Figure 1. More study is needed to determine the factors affecting plasma production on shorter time scales (see Figures 2 and 3).

Table 1. Coefficients of Cosine Fit

Radial Bin	A	ϕ (deg)	C	Uncertainty
≤3.25 R_S	63.9 cm^{-3}	21.9 ± 27	94.0 cm^{-3}	24.7 cm^{-3}
3.5 ± 0.25 R_S	30.0 cm^{-3}	9.3 ± 33	65.9 cm^{-3}	13.0 cm^{-3}
4.0 ± 0.25 R_S	21.5 cm^{-3}	22.6 ± 38	74.6 cm^{-3}	10.8 cm^{-3}
4.5 ± 0.25 R_S	10 cm^{-3}	***	73 cm^{-3}	10 cm^{-3}
5.0 ± 0.25 R_S	4 cm^{-3}	***	65 cm^{-3}	5 cm^{-3}

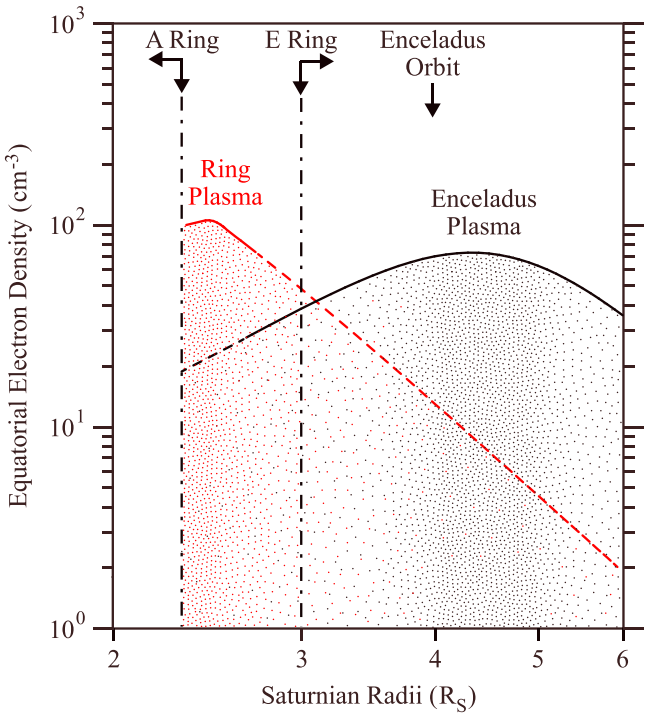

Figure 7. An illustration of the merging and mixing of the two primary plasma populations in the region between the outer edge of the A Ring and the orbit of Enceladus. The solid black line reproduces the power law fit in Figure 1, and the solid red line traces the inbound SOI density profile from Figure 1. The ring plasma (red) peaks in the region just beyond the outer edge of the A Ring and falls off with increasing distance from Saturn. The Enceladus plasma (black) has a broad peak between 4 R_s and 5 R_s, with densities falling off both inward and outward from the peak density region. The illustration shows that the Enceladus plasma dominates in the region beyond the Enceladus orbit and the ring plasma dominates in the region just outside the A Ring.

4. Summary

The waning of the seasonal variation in the inner magnetospheric plasma with increasing distance from Saturn suggests that the ring plasma expands radially outward from the main rings and over the E Ring, becoming a small component of the magnetospheric plasma population beyond 4 R_s, where the Enceladus plasma component dominates. Because of the strong dust-plasma absorption in the ring ionosphere, the bulk of the ring plasma expanding radially outward is generated in the region just beyond the A Ring by the photoionization of oxygen and hydrogen molecules scattered into the extended ring atmosphere just beyond the outer edge of the A Ring. The second plasma component in this region has its source in the icy particles venting from Enceladus' southern polar region. The decomposition of these particles and subsequent ionization creates the Enceladus plasma which diffuses both outward and inward toward the A Ring. The Enceladus plasma has no known seasonal dependence. In the inner magnetosphere, the two plasma populations merge. Figure 7 illustrates the merging and mixing of these two plasma populations in the region between the A Ring and the orbit of Enceladus. The solid black line reproduces the power law fit for the equatorial electron density measurements in Figure 1, and the solid red line traces the inbound SOI equatorial density profile from Figure 1. The dashed lines are extrapolations in the regions where density measurements are not available. The Enceladus plasma (black) peaks between 4 R_s and 5 R_s [*Persoon et al.*, 2013] and rolls off inside 4 R_s as the plasma diffuses inward toward the A Ring. The ring plasma (red) peaks just beyond the outer edge of the A Ring at 2.4 R_s and falls off with increasing radial distance from Saturn.

Enceladus is the dominant plasma source in Saturn's magnetosphere. Plasma created through the ionization of water group neutrals from Enceladus' plumes dominates the total plasma population in the region beyond Enceladus. The seasonally dependent ring plasma peaks in the source region just outside the A Ring and, at least near summer solstice, is likely to have peak densities comparable to the peak densities measured at Enceladus. The SOI density measurements, taken near the outer edge of the A Ring less than 2 years past the southern summer solstice, are very high, on the order of the highest densities at Enceladus (see Figure 1). Electron densities are currently increasing again as Cassini moves toward the northern summer solstice in May 2017. Just 9 months before the northern summer solstice, Cassini will return to the region just beyond the A Ring in a series of high inclination orbits near the F Ring and will likely encounter high ring plasma densities again.

Acknowledgments
The Cassini RPWS data through day 298, 2014 are in the Planetary Data System. More recent data can be requested from the lead author of this paper. This research was supported by NASA through contract 1415150 with the Jet Propulsion Laboratory.

Michael Liemohn thanks the reviewers for their assistance in evaluating this paper.

References

Arridge, C. S., et al. (2012), Mapping magnetospheric equatorial regions at Saturn from Cassini prime mission observations, *Space Sci. Rev.*, *164*, 1–83, doi:10.1007/s11214-011-9850-4.

Bouhram, M., R. E. Johnson, J.-J. Berthelier, J.-M. Illiano, R. L. Tokar, D. T. Young, and F. J. Crary (2006), A test-particle model of the atmosphere/ionosphere system of Saturn's main rings, *Geophys. Res. Lett.*, *33*, L05106, doi:10.1029/2005GL025011.

Carlson, R. W. (1980), Photo-sputtering of ice and hydrogen around Saturn's rings, *Nature*, *283*, 461, doi:10.1038/283461a0.
Cassidy, T. A., and R. E. Johnson (2010), Collisional spreading of Enceladus' neutral cloud, *Icarus*, *209*, 696–695, doi:10.1016/j.icarus.2010.04.010.
Coates, A. J., et al. (2005), Plasma electrons above Saturn's main rings: CAPS observations, *Geophys. Res. Lett.*, *32*, L14S09, doi:10.1029/2005GL022694.
Dougherty, M. K., K. K. Khurana, F. M. Neubauer, C. T. Russell, J. Saur, J. S. Leisner, and M. E. Burton (2006), Identification of a dynamic atmosphere at Enceladus with the Cassini magnetometer, *Science*, *311*, 1406–1409, doi:10.1126/science.1120985.
Elrod, M. K., W.-L. Tseng, A. K. Woodson, and R. E. Johnson (2014), Seasonal and radial trends in Saturn's thermal plasma between the main rings and Enceladus, *Icarus*, *242*, 130–137, doi:10.1016/j.icarus.2014.07.020.
Esposito, L. W., M. O'Callaghan, K. E. Simmons, C. W. Hord, R. A. West, A. L. Lane, R. B. Pomphrey, D. L. Coffeen, and M. Sato (1983), Voyager photopolarimeter stellar occultation of Saturn's rings, *J. Geophys. Res.*, *88*, 8643–8649, doi:10.1029/JA088iA11p08643.
Farmer, A. J. (2009), Saturn in hot water: Viscous evolution of the Enceladus torus, *Icarus*, *202*, 280–286, doi:10.1016/j.icarus.2009.02.031.
Farrell, W. M., M. L. Kaiser, D. A. Gurnett, W. S. Kurth, A. M. Persoon, J. E. Wahlund, and P. Canu (2008), Mass unloading along the inner edge of the Enceladus plasma torus, *Geophys. Res. Lett.*, *35*, L02203, doi:10.1029/2007GL032306.
Frank, L. A., B. G. Burek, K. L. Ackerson, J. H. Wolfe, and J. D. Mihalov (1980), Plasmas in Saturn's magnetosphere, *J. Geophys. Res.*, *85*, 5695–5708, doi:10.1029/JA085iA11p05695.
Gurnett, D. A., et al. (2005), Radio and plasma wave observations at Saturn from Cassini's approach and first orbit, *Science*, *307*, 1255–1259, doi:10.1126/science.1105356.
Hansen, C. J., L. Esposito, A. I. F. Stewart, J. Colwell, A. Hendrix, W. Pryor, D. Shemansky, and R. West (2006), Enceladus' water vapor plume, *Science*, *311*, 1422–1425, doi:10.1126/science.1121254.
Hartogh, P., et al. (2011), Direct detection of the Enceladus water torus with Herschel, *Astron. Astrophys.*, *532*, L2, doi:10.1051/0004-6361/201117377.
Holmberg, M. K. G., J.-E. Wahlund, M. W. Morooka, and A. M. Persoon (2012), Ion densities and velocities in the inner plasma torus of Saturn, *Planet. Space Sci.*, *73*, 151–160, doi:10.1016/j.pss.2012.09.016.
Ip, W.-H. (1995), The exospheric systems of Saturn's rings, *Icarus*, *115*, 295–303, doi:10.1006/icar.1995.1098.
Ip, W.-H. (2005), An update on the ring exosphere and plasma disc of Saturn, *Geophys. Res. Lett.*, *32*, L13204, doi:10.1029/2004GL022217.
Johnson, R. E., M. K. Pospieszalska, E. C. Sittler Jr., A. F. Cheng, L. J. Lanzerotti, and E. M. Sieveka (1989), The neutral cloud and heavy ion inner torus at Saturn, *Icarus*, *77*, 311–329, doi:10.1016/0019-1035(89)90092-4.
Johnson, R. E., et al. (2006a), Production, ionization and redistribution of O_2 in Saturn's ring atmosphere, *Icarus*, *180*, 393–402, doi:10.1016/j.icarus.2005.08.021.
Johnson, R. E., H. T. Smith, O. J. Tucker, M. Liu, M. H. Burger, E. C. Sittler, and R. L. Tokar (2006b), The Enceladus and OH tori at Saturn, *Astrophys. J.*, *644*, L137–L139, doi:10.1086/505750.
Jurac, S., and J. D. Richardson (2005), A self-consistent model of plasma and neutrals at Saturn: Neutral cloud morphology, *J. Geophys. Res.*, *110*, A09220, doi:10.1029/2004JA010635.
Jurac, S., R. E. Johnson, and J. D. Richardson (2001), Saturn's E ring and production of the neutral torus, *Icarus*, *149*, 384–396, doi:10.1006/icar.2000.6528.
Jurac, S., M. A. McGrath, R. E. Johnson, J. D. Richardson, V. M. Vasyliunas, and A. Eviatar (2002), Saturn: Search for a missing water source, *Geophys. Res. Lett.*, *29*(24, 2172), doi:10.1029/2002GL015855.
Morfill, G. E., H. Fechtig, E. Gruen, and C. K. Goertz (1983), Some consequences of meteoroid impacts on Saturn's rings, *Icarus*, *55*, 439–447, doi:10.1016/0019-1035(83)90114-8.
Morooka, M. W., et al. (2009), The electron density of Saturn's magnetosphere, *Ann. Geophys.*, *27*, 2971–2991, doi:10.5194/angeo-27-2971-2009.
Persoon, A. M., D. A. Gurnett, W. S. Kurth, G. B. Hospodarsky, J. B. Groene, P. Canu, and M. K. Dougherty (2005), Equatorial electron density measurements in Saturn's inner magnetosphere, *Geophys. Res. Lett.*, *32*, L23105, doi:10.1029/2005GL024294.
Persoon, A. M., D. A. Gurnett, W. S. Kurth, and J. B. Groene (2006), A simple scale height model of the electron density in Saturn's plasma disk, *Geophys. Res. Lett.*, *33*, L18106, doi:10.1029/2006GL027090.
Persoon, A. M., et al. (2009), A diffusive equilibrium model for the plasma density in Saturn's magnetosphere, *J. Geophys. Res.*, *114*, A04211, doi:10.1029/2008JA013912.
Persoon, A. M., D. A. Gurnett, J. S. Leisner, W. S. Kurth, J. B. Groene, and J. B. Faden (2013), The plasma density distribution in the inner region of Saturn's magnetosphere, *J. Geophys. Res. Space Physics*, *118*, 2970–2974, doi:10.1002/jgra.50182.
Porco, C. C., et al. (2006), Cassini observes the active south pole of Enceladus, *Science*, *311*, 1393–1401, doi:10.1126/science.1123013.
Pospieszalska, M. K., and R. E. Johnson (1991), Micrometeorite erosion of the main rings as a source of plasma in the inner Saturnian plasma torus, *Icarus*, *93*, 45–52, doi:10.1016/0019-1035(91)90162-M.
Richardson, J. D., A. Eviatar, M. A. McGrath, and V. M. Vasyliunas (1998), OH in Saturn's magnetosphere: Observations and implications, *J. Geophys. Res.*, *103*, 20,245–20,255, doi:10.1029/98JE01127.
Schippers, P., et al. (2008), Multi-instrument analysis of electron populations in Saturn's magnetosphere, *J. Geophys. Res.*, *113*, A07208, doi:10.1029/2008JA013098.
Schippers, P., M. Moncuquet, N. Meyer-Vernet, and A. Lecacheux (2013), Core electron temperature and density in the innermost Saturn's magnetosphere from HF power spectra analysis on Cassini, *J. Geophys. Res. Space Physics*, *118*, 7170–7180, doi:10.1002/2013JA019199.
Shemansky, D. E., P. Matheson, D. T. Hall, H.-Y. Hu, and T. M. Tripp (1993), Detection of the hydroxyl radical in the Saturn magnetosphere, *Nature*, *363*, 329–331, doi:10.1038/363329a0.
Shi, M., R. A. Baragiola, D. E. Grosjean, R. E. Johnson, S. Jurac, and J. Schou (1995), Sputtering of water ice surfaces and the production of extended neutral atmospheres, *J. Geophys. Res.*, *100*, 26,387–26,395, doi:10.1029/95JE03099.
Sittler, E. C., Jr., et al. (2008), Ion and neutral sources and sinks within Saturn's inner magnetosphere: Cassini results, *Planet. Space Sci.*, *56*, 3–18, doi:10.1016/j.pss.2007.06.006.
Tokar, R. L., et al. (2005), Cassini observations of the thermal plasma in the vicinity of Saturn's main rings and the F and G rings, *Geophys. Res. Lett.*, *32*, L14S04, doi:10.1029/2005GL022690.
Tseng, W.-L., W.-H. Ip, R. E. Johnson, T. A. Cassidy, and M. K. Elrod (2010), The structure and time variability of the ring atmosphere and ionosphere, *Icarus*, *206*, 382–389, doi:10.1016/j.icarus.2009.05.019.
Tseng, W.-L., R. E. Johnson, M. F. Thomsen, T. A. Cassidy, and M. K. Elrod (2011), Neutral H_2 and H_2^+ ions in the Saturnian magnetosphere, *J. Geophys. Res.*, *116*, A03209, doi:10.1029/2010JA016145.
Wahlund, J.-E., et al. (2005), The inner magnetosphere of Saturn: Cassini RPWS cold plasma results from the first encounter, *Geophys. Res. Lett.*, *32*, L20S09, doi:10.1029/2005GL022699.

Waite, J. H., Jr., et al. (2005), Oxygen ions observed near Saturn's A ring, *Science*, *307*, 1260–1262, doi:10.1126/science1105734.
Waite, J. H., Jr., et al. (2006), Cassini Ion and Neutral Mass Spectrometer: Enceladus plume composition and structure, *Science*, *311*, 1419–1422, doi:10.1126/science.1121290.
Wilson, G. R., and J. H. Waite Jr. (1989), Kinetic modeling of the Saturn ring-ionosphere plasma environment, *J. Geophys. Res.*, *94*(A12), 17,287–17,298, doi:10.1029/JA094iA12p17287.
Young, D. T., et al. (2005), Composition and dynamics of plasma in Saturn's magnetosphere, *Science*, *307*, 1262–1265, doi:10.1126/science.1106151.